Phase Equilibria in the La-Me-Co-O (Me=Ca, Sr, Ba) Systems

V.A. Cherepanov[1], L.Ya. Gavrilova[1], L.Yu. Barkhatova[1], V.I. Voronin[2], M.V. Trifonova[1] and O.A. Bukhner[1]

[1]Department of Chemistry, Ural State University, Lenin av., 51, Yekaterinburg, 620083, Russia

[2]Institute for Metal Physics, Ural Branch of RAS, S. Kovalevskaya st., 18, Yekaterinburg, GSP-170, 620219, Russia

Abstract. The phase equilibria of the La-Me-Co-O systems (Me = Ca, Sr and Ba) were studied in air at 1100 °C. Two types of solid solution of general composition $La_{1-x}Me_xCoO_{3-\delta}$ and $(La_{1-y}Me_y)_2CoO_4$ were found to exist in the systems. The limiting composition of $La_{1-x}Me_xCoO_{3-\delta}$ lies at x = 0.8 for Me = Sr, Ba and between 0.3-0.5 for Me = Ca. It is shown that the rhombohedral distortion of the perovskite type $La_{1-x}Me_xCoO_{3-y}$ decreases while x increases. $La_{1-x}Me_xCoO_{3-\delta}$ (Me = Sr, Ba) shows an ideal cubic structure at x = 0.5. The stability range of $(La_{1-y}Me_y)_2CoO_4$ was found to be $0.25 \leq y \leq 0.35$ for Me = Ca, $0.3 \leq y \leq 0.55$ for Me = Sr and $0.3 \leq y \leq 0.375$ for Me = Ba. All phases have tetragonal K_2NiF_4-type crystal structure. Based on the XRD and neutron diffraction patterns of quenched samples, the phase diagrams (Gibbs triangles) are constructed for all systems. The phase equilibrium at low oxygen pressure is shown for the example of the La-Sr-Co-O system. The decomposition mechanism of $La_{1-x}Sr_xCoO_{3-\delta}$ at 1100 °C for the samples with $0.5 < x < 0.8$ within the oxygen pressure range $-0.678 > \log(Po_2) > -2.25$ can be written as follows: $La_{1-x'}Sr_{x'}CoO_{3-\delta'} = n\ La_{1-x''}Sr_{x''}CoO_{3-\delta''} + m\ SrCoO_{2.5} + q/2\ O_2$ where $x' > x''$. The decomposition mechanism of $La_{1-x}Sr_xCoO_{3-\delta}$ for the samples with $x < 0.5$ within the oxygen pressure range $-2.25 > \log(Po_2) > -3.55$ changes and can be written as follows: $La_{1-x}Sr_xCoO_{3-\delta'} = r\ La_{1-x'}Sr_{x'}CoO_{3-\delta''} + w\ (La_{1-y'}Sr_{y'})_2CoO_4 + \nu\ CoO + f/2\ O_2$. The results are shown in "$\log Po_2$-composition" diagrams.

1. Introduction

Alkali earth substituted lanthanum cobaltates with the perovskite-type structure have received considerable attention in recent years due to their potential application as electrodes, catalysts, membranes etc. Successful use of any material in the wide range of temperature and pressure require detailed knowledge of the stability boundaries of the phases and the phase equilibria. However, a number of papers concerning the synthesis procedure, crystal and electronic structure, catalytic activity and magnetic properties [1-8] do not give much information about phase equilibria and stability ranges of the single phases in the systems. Such phase equilibria data are usually given by the appropriate phase diagrams. The phase equilibria of quasibinary systems were studied earlier: La-Co-O system in [9-12], Me-Co-O systems (Me= Ca, Sr, Ba) in [13-15], La-Me-O systems in [15]. In this study, we will represent the phase diagrams of La-Me-Co-O systems (Me = Ca, Sr and Ba) at 1100 °C in air. The phase equilibria at low oxygen pressure will be shown for the example of the La-Sr-Co-O system.

2. Experimental Methods

Lanthanum oxide La_2O_3 (99.99 % purity), alkali earth metal carbonates $MeCO_3$ and cobalt oxide Co_3O_4, all of "pure for analysis" or "special purity" grade were used as starting materials. All of them were initially annealed: La_2O_3 at 1200 °C, $MeCO_3$ at 500-700 °C, Co_3O_4 at 700 °C. The samples for investigation (except some special cases, which will be described later) were prepared by mixing the starting materials in appropriate ratios. The mixtures were grinded in an agate mortar and fired in air at

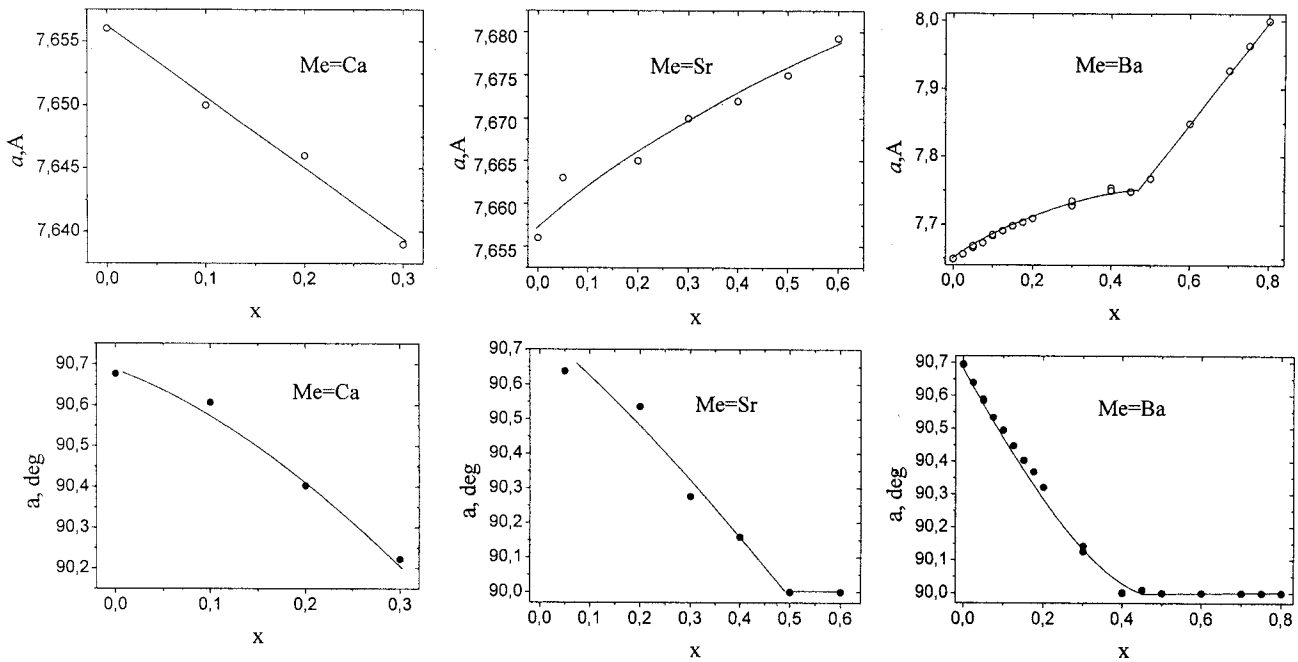

Fig. 1. Pseudocubic unit cell parameters of $La_{1-x}Me_xCoO_{3-\delta}$.

850 °C for 24 hrs., at 950 °C for 24 hrs. and finally at 1100 °C for 70-400 hrs. with intermediate grinding in alcohol after every 24 hrs. After each stage the samples were quenched to room temperature on a cold massive copper plate. A number of samples was fired later at 1100 °C in atmospheres with different oxygen partial pressures for 24-100 hrs. It was performed in a special cell which kept and controlled the required constant oxygen partial pressure and temperature over long periods of time. The samples were quenched finally under constant Po_2. In order to identify the phase composition, all samples were examined by X-ray diffraction, using a DRON-3 diffractometer with Cu-K_α radiation or Guinier camera with Cu-$K_{\alpha 1}$ radiation. The equilibrium state was considered to be reached when the phase composition (i.e. X-ray patterns) remained unchanged during a few last stages of firing. In some cases, powder neutron diffraction experiments were made to determine the crystal structure of the single phases. Powder neutron profiles were measured at the research reactor IVV-2, located near Ekaterinburg, Russia, on the D7A diffractometer with a double monochromator - (002) reflection of a single crystal of pyrolytic graphite and (333) reflection of germanium. The wavelength employed was 1.515 Å. Collected data were refined by the Rietveld profile method using the "DBWS4911" and "Fullpof" programs.

Due to the fact that the oxygen content and oxidation state of the cobalt ions change as a function of the metal ratio, a composition in the phase diagram is represented as a relative mole fraction of the metal content, for example $\xi_{Co} = n_{Co}/(n_{La}+n_{Me}+n_{Co})$. The oxygen content in the solid phases has not been taken into account.

3. Results and Discussion

3.1. Phase Diagrams of La-Me-Co-O Systems at 1100 °C in Air. The only phases found in all quasiternary systems were $La_{1-x}Me_xCoO_{3-\delta}$ and $(La_{1-y}Me_y)_2CoO_4$. All attempts to substitute the lanthanum ions for alkali earth ion in $La_4Co_3O_{10}$ failed at least in air at 1100 °C.

The homogeneity range of $La_{1-x}Me_xCoO_{3-\delta}$ in air at 1100 °C was found to be $0 \le x \le 0.8$ for Me = Sr, Ba and $0 \le x \le 0.3$ for Me = Ca. In all cases the rhombohedral distortions of perovskite-type $La_{1-x}Me_xCoO_{3-\delta}$ (space group $R\bar{3}c$) decrease while the alkali earth metal content increases; however, the unit cell parameter a decrease for Me = Ca and increases for Me = Sr and Ba. In both Sr and Ba substituted cobaltates the unit cell became ideal cubic at x = 0.5. The parameters of the pseudocubic unit cell of $La_{1-x}Me_xCoO_{3-\delta}$ samples quenched from 1100 °C in air are shown in Fig. 1. All solid solutions with perovskite-type structure were oxygen deficient oxides. The value of

Table 1. The unit cell parameters of $(La_{1-y}Me_y)_2CoO_4$

Me	composition (y)	a, Å	c, Å
Ca	0.25	3.8188(7)	12.304(2)
	0.30	3.8143(7)	12.285(2)
Sr	0.300	3.8305(1) 3.8285(1)*	12.5184(2) 12.5169(1)*
	0.312	3.8296(1)	12.5131(2)
	0.325	3.8175(1)	12.5046(5)
	0.350	3.8095(3)	12.489(1)
	0.400	3.8160(1) 3.8161(2)*	12.4803(1) 12.4833(8)*
	0.500	3.8056(1) 3.8026(2)*	12.4942(3) 12.488(1)*
	0.525	3.8019(1)	12.4986(3)
Ba	0.300	3.8565(7)	12.812(5)
	0.325	3.8544(1)	12.805(1)
	0.350	3.8539(1)	12.817(1)
	0.375	3.8506(2)	12.820(1)

*Results, obtained from the neutron diffraction measurements.

oxygen deficiency slightly increases from Ca- to Ba-substituted lanthanum cobaltate.

$La_2Co^{2+}O_4$ could not be obtained in air [9-12]. However, partial substitution of La^{3+} ions for Me^{2+} increased the average oxidation state of the cobalt ions in $(La_{1-y}Me_y)_2CoO_4$. Single phase samples of $(La_{1-y}Me_y)_2CoO_4$ composition were obtained within the range $0.25 \le y \le 0.35$ for Me = Ca; $0.30 \le y \le 0.55$ for Me=Sr and $0.300 \le y \le 0.375$ for Me = Ba. All of them had tetragonal K_2NiF_4-type structure. The unit cell parameters are listed in Table 1. According to the results of neutron diffraction measurements at least Sr- and Ba-substituted $(La_{1-y}Me_y)_2CoO_4$ solid solutions have their oxygen content close to stoichiometric composition for all values of y.

It should be noted that the time required for preparation of single phase or equilibrium samples in La-Ca-Co-O system was much longer than in the case of Sr- or Ba-substituted systems.

La-Ca-Co-O system. Samples of the overall composition $La_{1-x}Ca_xCoO_{3-\delta}$ with x = 0.1, 0.2, 0.3, 0.4, 0.5 and 0.6 were annealed at 1100 °C in air. The samples with x = 0.1 and 0.2 show single phases after 150 hours, the sample with x = 0.3 after 300 hours. The samples with $x \ge 0.4$ remained multiphases even after 480 hours of firing. The samples with x = 0.4 and 0.5 can be easily obtained as single phases at every stage at 1100 °C by annealing them in pure oxygen for 20 hours. These facts and phase composition of some other samples (between $La_{1-x}Ca_xCoO_{3-\delta}$ and $(La_{1-y}Ca_y)_2CoO_4$ inside the Gibbs triangle) led as to the conclusion that the homogeneity range of $La_{1-x}Ca_xCoO_{3-\delta}$ have to be somewhere between x = 0.3 and 0.4. at 1100 °C in air.

The XRD patterns of the $(La_{1-y}Ca_y)_2CoO_4$ samples with y = 0.15, 0.2, 0.3, 0.35, 0.4, 0.45, 0.5, 0.6 and 0.8 show that the formation of the $(La_{1-y}Ca_y)_2CoO_4$ phase has taken place; however, none of the samples has been obtained as a single phase even after 500 hours of firing at 1100 °C in air. It should be noted that during the last stages the samples with y = 0.8, 0.6 and 0.5 look as if they reached their equilibrium state, whereas those with $y \le 0.4$ slowly changed from stage to stage. In order to accelerate the process of synthesis some of the compositions were prepared by the coprecipitation method. For this purpose, La_2O_3, $CaCO_3$ and Co (obtained by reducing of CoO in the flux of hydrogen at 400 °C) mixed in appropriate ratios were dissolved in concentrated hot HCl. Coprecipitation was achieved by the addition of 20 % KOH solution. Precipitations were left for a couple of days for recrystallization. Then, they were filtered and washed by a large amount of water until full removal of Cl^- ions. Then, the coprecipitated samples were slowly heated up to 1100 °C (with intermediate grindings). After 120 hours firing at 1100 °C the samples with y = 0.25 and 0.30 became single phases.

The existence of La_2CaO_χ as a single phase for the conditions under investigation is confirmed. XRD data were in good agreement with [16].

Based on the results of XRD patterns of about 40 samples the Gibbs triangle was divided into 9 fields. The phase diagram of the La-Ca-Co-O system at 1100 °C in air is shown in Fig. 2. The regions of limited solubility of CaO in CoO and vice versa are shown as reported in [13].

La-Sr-Co-O System. Single phase samples of $La_{1-x}Sr_xCoO_{3-\delta}$ with $0 \le x \le 0.8$ and $(La_{1-y}Sr_y)_2CoO_4$ with $0.3 \le y \le 0.55$ can be obtained after 60-150 hours of firing at 1100 °C in air. All samples of $La_{1-x}Sr_xCoO_{3-\delta}$ with compositions of x > 0.8, starting from x = 0.825 were found to be mixtures of Sr-saturated perovskite phase and $Sr_2Co_2O_5$. The process of $La_{1-x}Sr_xCoO_{3-\delta}$ synthesis occurred via $LaCoO_3$ (or $La_{1-x}Sr_xCoO_{3-\delta}$ with a small value of x) and $Sr_2Co_2O_5$ as intermediate products. In further stages they interacted forming single phase $La_{1-x}Sr_xCoO_{3-\delta}$

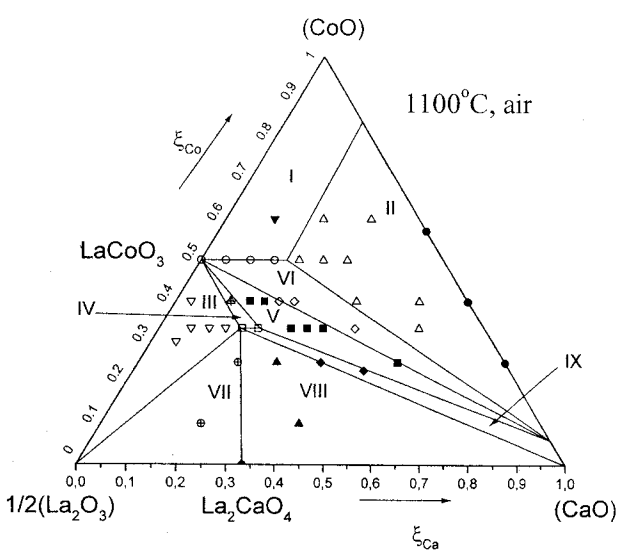

Fig. 2. The phase diagram of La-Ca-Co-O system at 1100 °C in air. The phase composition in the fields are: I - $La_{1-x}Ca_xCoO_3$ + solid solution of CaO in CoO; II - saturated solid solution of CaO in CoO + saturated solid solution of CoO in CaO + Ca-saturated $La_{1-x}Ca_xCoO_{3-\delta}$; III - La_2O_3 + $LaCoO_{3-\delta}$ + limiting composition (Ca-poor) of $(La_{1-y}Ca_y)_2CoO_4$; IV - $LaCoO_{3-\delta}$ + $(La_{1-y}Ca_y)_2CoO_4$; V - $LaCoO_{3-\delta}$ + limiting composition (Ca-rich) of $(La_{1-y}Ca_y)_2CoO_4$ + saturated solid solution of CoO in CaO; VI - saturated solid solution of CoO in CaO + $La_{1-x}Ca_xCoO_{3-\delta}$; VII - La_2O_3 + La_2CaO_x + limiting composition (Ca-poor) of $(La_{1-y}Ca_y)_2CoO_4$; VIII - La_2CaO_x + limiting composition (Ca-poor) of $(La_{1-y}Ca_y)_2CoO_4$ + CaO; IX - $(La_{1-x}Ca_x)_2CoO_4$ + solid solution of CoO in CaO.

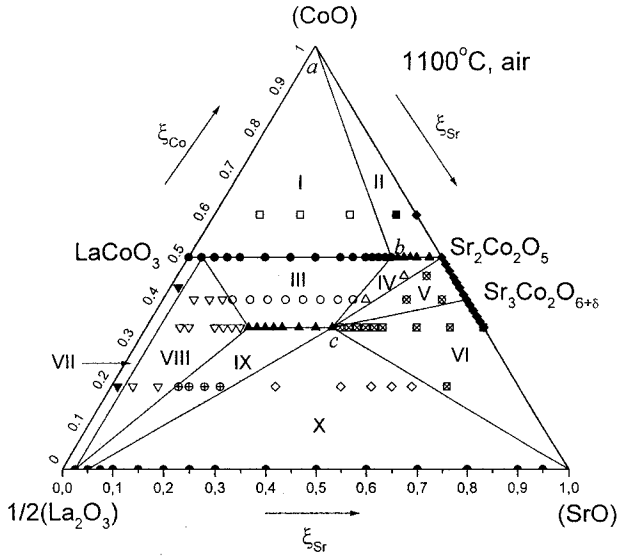

Fig. 3. The phase diagram of La-Sr-Co-O system at 1100 °C in air. The phase composition in the fields are: I - CoO + $La_{1-x}Sr_xCoO_{3-\delta}$; II - CoO + $La_{0.2}Sr_{0.8}CoO_{3-\delta}$ + $Sr_2Co_2O_5$; III - $La_{1-x}Sr_xCoO_{3-\delta}$+$(La_{1-y}Sr_y)_2CoO_4$; IV - $La_{0.2}Sr_{0.8}CoO_{3-\delta}$+ $(La_{0.45}Sr_{0.55})_2CoO_4$ + $Sr_2Co_2O_5$; V - $(La_{0.45}Sr_{0.55})_2CoO_4$ + $Sr_2Co_2O_5$ + $Sr_3Co_2O_{6+\delta}$; VI - $(La_{0.45}Sr_{0.55})_2CoO_4$ + $Sr_3Co_2O_{6+\delta}$ + SrO; VII - La_2O_3-SrO solid solution + $La_{1-x}Sr_xCoO_{3-\delta}$ ($0 \le x \le 0.06$); VIII - $La_{0.95}Sr_{0.05}CoO_{3-\delta}$ + $(La_{0.7}Sr_{0.3})_2CoO_4$ + La_2O_3-SrO solid solution with fixed composition; IX - La_2O_3-SrO solid solution + $(La_{1-y}Sr_y)_2CoO_4$; X - $(La_{0.45}Sr_{0.55})_2CoO_4$ + La_2O_3-SrO solid solution with fixed composition + SrO.

The samples of $(La_{1-y}Sr_y)_2CoO_4$ with the composition of $y < 0.3$ were mixtures of $(La_{0.7}Sr_{0.3})_2CoO_4$, $La_{1-x'}Sr_{x'}CoO_{3-\delta}$ with $x' \approx 0.06$ and La_2O_3-SrO solid solution with fixed composition within the composition range $0 < \xi_{Sr} < 0.05$. The samples with $x > 0.55$ were mixtures of Sr-saturated $(La_{0.7}Sr_{0.3})_2CoO_4$, $Sr_3Co_2O_{6+\delta}$ and SrO.

An existence of $Sr_2Co_2O_5$ and $Sr_3Co_2O_{6+\delta}$ as single phases in the conditions under investigation is confirmed. XRD data were in good agreement with [17,18].

Based on the results of XRD patterns of about 70 samples, the Gibbs triangle was divided into 10 fields. The phase diagram of the La-Sr-Co-O system at 1100 °C in air is shown in Fig. 3.

La-Ba-Co-O System. Preparation of single phase samples of $(La_{1-y}Ba_y)_2CoO_4$ with compositions of $0.3 \le y \le 0.375$ took, similarly to the Sr-containing system, about 100-150 hours of firing at 1100 °C in air. The time required to synthesize $La_{1-x}Ba_xCoO_{3-\delta}$ single phase with $0 \le x \le 0.8$ depended strongly on the composition (x). Preparation of the single phase samples with $x \le 0.4$ took about 50-70 hours at 1100 °C, while for $0.65 \le x \le 0.8$ 100-200 hours were necessary. Main difficulties arose for the preparation of single phase samples with $0.45 \le x \le 0.6$. XRD patterns from different stages of firing show that at first stages a mixture of phases of $La_{1-x}Ba_xCoO_{3-\delta}$ with small and large values of x were formed. Coexistence of these phases is easily determined because of the considerable difference in lattice parameter. Further annealing led to equalization of the Ba content in coexisting phases. Only after a series of annealing of a total time of 500-600 hours the samples with $0.45 \le x \le 0.6$ were transformed to single phases.

Special attention has been paid to the ability of Ba-substituted lanthanum cobaltate to be nonstoichiometric in the metal ion sublattices reported for $La_{0.7-x}Sr_{0.3}CoO_3$ ($x_{max} = 0.15$) [19]. Precise X-ray and neutron diffraction showed that all samples with "$La_{0.8-x}Ba_{0.2}CoO_{3-\delta}$" ($x = 0.02, 0.05, 0.07, 0.10$ and 0.13) and "$La_{0.6-x}Ba_{0.4}CoO_{3-\delta}$" ($x = 0.02, 0.05, 0.07, 0.10$) as nominal compositions were mixtures of $La_{1-x}Ba_xCoO_{3-\delta}$ and CoO. Therefore, it was concluded that the La deficit in $La_{1-x}Ba_xCoO_{3-\delta}$, if it is possible, did not exceed 0.02. The smallest deviation of stoichiometry in the metals ratio towards the enrichment of either lanthanum or barium (strontium) always led to

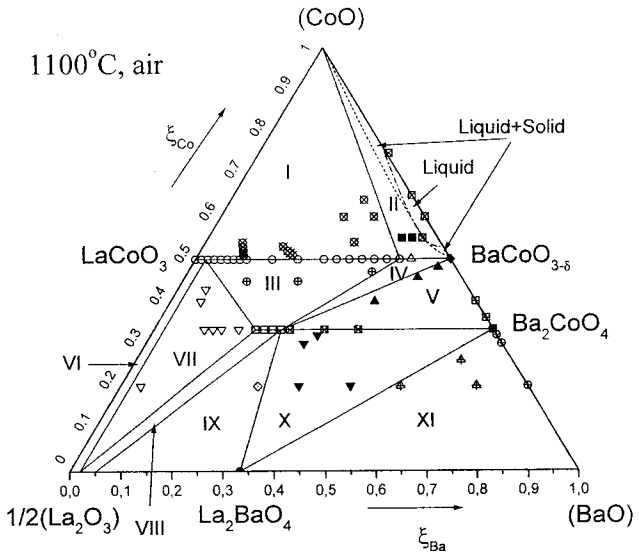

Fig. 4. The phase diagram of La-Ba-Co-O system at 1100 °C in air. The phase composition in the fields are: I - $La_{1-x}Ba_xCoO_{3-\delta}$ + CoO; II - $La_{0.2}Ba_{0.8}CoO_{3-\delta}$ + CoO + $BaCoO_{3-\delta}$ III - $La_{1-x}Ba_xCoO_{3-\delta}$ ($0.06 \le x \le 0.8$) + $(La_{1-y}Ba_y)_2CoO_4$ ($0.3 \le y \le 0.375$); IV - $La_{0.2}Ba_{0.8}CoO_{3-\delta}$ + $(La_{0.625}Ba_{0.375})_2CoO_4$ + $BaCoO_{3-\delta}$; V - $(La_{0.625}Ba_{0.375})_2CoO_4$ + $BaCoO_{3-\delta}$ + Ba_2CoO_4;. VI - $La_{1-x}Ba_xCoO_{3-\delta}$ ($0 \le x < 0.06$) + La_2O_3-BaO solid solution; VII - $La_{0.94}Ba_{0.06}CoO_{3-\delta}$ + $(La_{0.7}Ba_{0.3})_2CoO_4$ + La_2O_3-BaO solid solution with fixed composition; VIII - $(La_{1-y}Ba_y)_2CoO_4$ ($0.3 \le y \le 0.375$) + La_2O_3-BaO solid solution; IX - La_2O_3-BaO solid solution + $(La_{0.625}Ba_{0.375})_2CoO_4$ + La_2BaO_4; X - $(La_{0.625}Ba_{0.375})_2CoO_4$ + La_2BaO_4 + Ba_2CoO_4; XI - La_2BaO_4 + Ba_2CoO_4 + BaO.

the formation of $(La_{1-y}Ba_y)_2CoO_4$ (or $(La_{1-y}Sr_y)_2CoO_4$ in the Sr-containing system).

The existence of La_2BaO_χ, $BaCoO_{3-\delta}$ and Ba_2CoO_χ as single phases under the conditions of investigation was confirmed. XRD data were in good agreement with [14, 20].

Based on the results of XRD patterns of about 80 samples, the Gibbs triangle was divided into 13 fields. The phase diagram of the La-Ba-Co-O system at 1100 °C in air is shown in Fig. 4.

Some Comparison of La-Me-Co-O Phase Diagrams

Lower solubility of calcium in $LaCoO_3$ in comparison with strontium and barium reflects in some sense the differences in the Ca-Ca-O and Sr (or Ba)-Co-O quasi-binary systems under the conditions of investigation: an absence of intermediate phases in the former and two ternary oxides in both later systems. On the other hand, smaller sized Ca ions do not allow to reach a high value of oxygen nonstoichiometry in $La_{1-x}Ca_xCoO_{3-\delta}$ which is increased together with Ca content.

A more narrow solubility range of Ca and Ba occured in comparison to Sr-substituted $(La_{1-y}Me_y)_2CoO_4$ caused by the existence of ternary oxides such as La_2CaO_4 and La_2BaO_4.

3.2. The Phase Equilibria of La-Sr-Co-O System at 1100 °C and Low Oxygen Pressure. The phase equilibria at 1100 °C in the atmospheres with low oxygen pressure were studied using the samples with ratios $(n_{La}+n_{Sr})/n_{Co} = 1$ and $(n_{La}+n_{Sr})/n_{Co} = 2$, or in other words, samples for which the overall composition can be written as $La_{1-x}Sr_xCoO_w$ and $(La_{1-y}Sr_y)_2CoO_u$.

The gradual decrease of oxygen pressure leads to an increase of the stratification region between $La_{1-x}Sr_xCoO_{3-\delta}$ and $Sr_2Co_2O_5$, i.e. it leads to the decrease of Sr content in $La_{1-x'}Sr_{x'}CoO_{3-\delta'}$ (where x' represents the limiting composition of solid solution at fixed T and Po_2, corresponding to the point "b" on the phase diagram, Fig. 3). During the first stages of oxygen pressure decrease ($-0.678 > \log(Po_2/atm) > -2.25$) the boundary of $La_{1-x}Sr_xCoO_{3-\delta}$ shifted towards $LaCoO_3$ according to the reaction:

$$La_{1-x'}Sr_{x'}CoO_{3-\delta'} = n\ La_{1-x''}Sr_{x''}CoO_{3-\delta''} + m/2\ Sr_2Co_2O_5 + q/2\ O_2 \quad (1)$$

where x' and x'' ($x > x'$) are limiting compositions of perovskite-type solid solution at Po_2' and Po_2'' respectively ($Po_2' > Po_2''$), $n=(1-x')/(1-x'')$, $m=(x'-x'')/(1-x'')$ and $q=(3-\delta')-(3-\delta'')n-xm$.

The decrease of oxygen partial pressure in this region did not affect much Sr-rich limiting composition of $(La_{1-y}Sr_y)_2CoO_4$ ($y \approx 0.55$ in air), although the decomposition reaction can be written as follows:

$$(La_{1-y'}Sr_{y'})_2CoO_4 = n'(La_{1-y''}Sr_{y''})_2CoO_4 + m'\ Sr_3Co_2O_{6+\delta} + k'/2\ O_2 \quad (2)$$

where y' and y'' ($y' > y''$) are limiting compositions of the K_2NiF_4-type solid solution at Po_2' and Po_2'' respectively ($Po_2' > Po_2''$), $n'=(1-y')/(1-y'')$, $m'=2(y'-y'')/\{3(1-y')\}$ and $k'=4-4n'-(6+\delta)m'$.

The changes of the value x' in the oxygen pressure region $-0.678 > \log(Po_2/atm) > -2.25$ was much larger in comparison with z'. Such dynamics of the changes of Sr-rich limiting compositions of $La_{1-x}Sr_xCoO_{3-\delta}$ and $(La_{1-y}Sr_y)_2CoO_4$ transformed to two-phase phase boundaries (shown in Fig. 3 as "ab" and "bc") into the straight line at

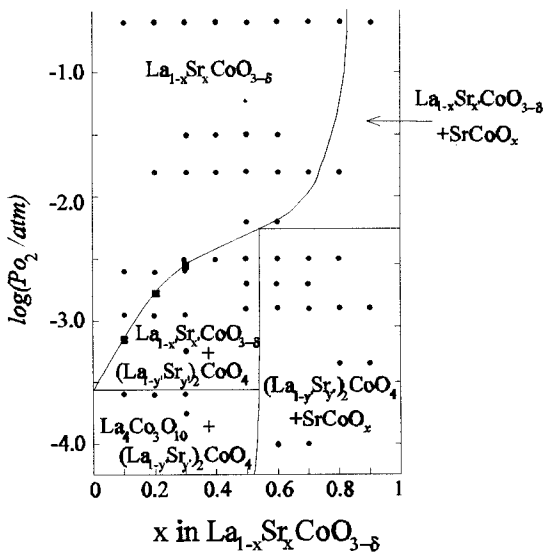

a

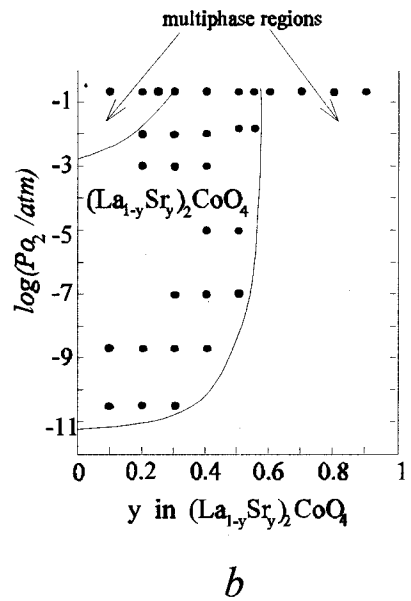

b

Fig. 5. The cross-sections of La-Sr-Co-O phase diagram: a) along $La_{1-x}Sr_xCoO_w$, b) along $(La_{1-y}Sr_y)_2CoO_u$.

$\log(Po_2/atm \approx -2.25$. It means that in this conditions x' = z' ≈ 0.5. The phase composition of each sample is shown in Fig. 5.

Further decrease of oxygen pressure (-2.25 > log (Po_2/atm) > -3.55) made y' > x'. This changed the general view of the phase diagram (Fig. 6) and produced a mechanism of $La_{1-x}Sr_xCoO_{3-\delta}$ decomposition:

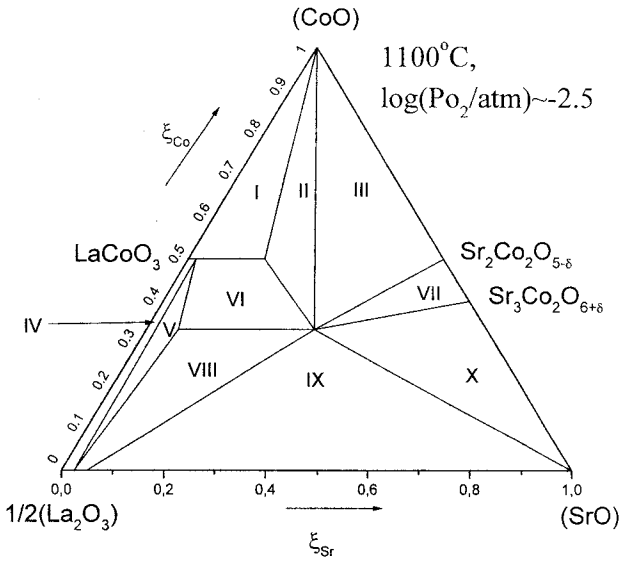

Fig. 6. The phase diagram of La-Sr-Co-O system at 1100 °C and log (Po_2/atm) = -2.5. The phase composition in the fields are: I - $La_{1-x}Sr_xCoO_{3-\delta}$ + CoO; II - Sr-saturated $La_{1-x'}Sr_{x'}CoO_{3-\delta}$ + Sr-saturated $(La_{1-y'}Sr_{y'})_2CoO_4$ + CoO; III - Sr-saturated $(La_{1-y'}Sr_{y'})_2CoO_4$ + $Sr_2Co_2O_{5-\delta}$ + CoO; IV - La_2O_3-SrO solid solution + $La_{1-x}Sr_xCoO_{3-\delta}$; V - La_2O_3-SrO solid solution with fixed composition + $La_{1-x}Sr_xCoO_{3-\delta}$ with fixed composition + limiting composition (Sr-poor) of $(La_{1-y'}Sr_{y'})_2CoO_4$; VI - $La_{1-x}Sr_xCoO_{3-\delta}$ + $(La_{1-y}Sr_y)_2CoO_4$; VII - Sr-saturated $(La_{1-y'}Sr_{y'})_2CoO_4$ + $Sr_2Co_2O_{5-\delta}$ + $Sr_3Co_2O_{6+\delta}$; VIII - La_2O_3-SrO solid solution + $(La_{1-y}Sr_y)_2CoO_4$; IX - Sr-saturated $(La_{1-y}Sr_y)_2CoO_4$ + La_2O_3-SrO solid solution with fixed composition + SrO; X - Sr-saturated $(La_{1-y}Sr_y)_2CoO_4$ + $Sr_3Co_2O_{6+\delta}$ + SrO.

$$La_{1-x'}Sr_{x'}CoO_{3-\delta'} = r\,La_{1-x''}Sr_{x''}CoO_{3-\delta''} + w(La_{1-y'}Sr_{y'})_2CoO_4 + \nu CoO + f/2\,O_2 \quad (3)$$

where x'=rx''+2wy', r+w+ν = 1 and f = 3-δ'-r(3-δ'')-4w-ν.

The Sr-poor limiting composition of $(La_{1-y}Sr_y)_2CoO_4$ y_{min} also changed while the oxygen pressure decreased. Its value strove to zero and it reached zero at Po_2 = 3.8 atm, where La_2CoO_4 appeared to be stable [11,12]. The thermodynamic stability range of $(La_{1-y}Sr_y)_2CoO_4$ as a function of Po_2 is shown in Fig. 5. It is not possible to specify all other multi-phase fields of this cross-section due to the difficulties in understanding of the Sr-Co-O phase equilibria at low oxygen pressure.

It should be noted that the reactions (1)-(3) do not represent exact thermodynamic equilibria. The left side of each equation represents an equilibrium composition at starting Po_2 and the final right side - equilibrium composition differs by infinitesimal lower Po_2.

4. Acknowledgements

This work has been supported in part by grants from the Russian Basic Science Foundation N 97-02-17315 and 97-03-33632 and Russian State Scientific and Technical Program "Neutron Investigation of Matter" NN96-104 and 96-305.

5. References

[1] C.N.R. Rao, Om Parkash, D. Bahadur, P. Ganguly and S. Nagabhushana, J. Solid State Chem. **22**, 353 (1977).

[2] I.F. Kononyuk, S.P. Tolochko, V.A. Lutsko and V.M. Anishchik, J. Solid State Chem. **48**, 209 (1983).

[3] H. Taguchi, M. Shimada and M. Koizumi, J. Solid State Chem. **44**, 254 (1982).

[4] H. Taguchi, M. Shimada and M. Koizumi, J. Solid State Chem. **41**, 329 (1982).

[5] S.P. Tolochko, I.F. Kononyuk and L.M. Lamekina, Zh. Neorganich. Khimii **28**, 1396 (1983).

[6] S.P. Tolochko, I.F. Kononyuk and S.F. Novik, Zh. Neorganich. Khimii **30**, 2079 (1985).

[7] T. Nakamura, M. Misono, Y. Yoneda, Bull. Chem. Soc. Japan **55**, 394 (1982).

[8] T. Nakamura, M. Misono, Y. Yoneda, J. Catal. **83**, 151 (1983).

[9] J.J. Janecek, G.P. Wirthz, J. Amer. Chem. Soc. **61**, 242 (1978).

[10] M. Seppanen, M. Kyto, P. Taskinen, Scand. J. Met. **8**, 199 (1979).

[11] A.N. Petrov, V.A. Cherepanov, E.M. Novitsky, V.M. Zhukovsky, Russian J. Phys. Chem. **58**, 2662 (1984).

[12] A.N. Petrov, V.A. Cherepanov, A.Yu. Zuev, V.M. Zhukovsky, J. Solid State Chem. **75**, 1 (1988).

[13] E. Woermann and A. Muan, J. Inorg. Nucl. Chem. **32**, 1455 (1970).

[14] T. Negas and R.S. Roth. Nat. Bur. Stand. Spec. Publ., Solid State Chem. Proc. 5th Mat. Res. Symp. **364**, 233 (1972).

[15] Phase Diagrams of the Systems of the Refractory Oxides. Reference Book. Ed. by Galakhov F.YA., Leningrad, Nauka, 1987, 284p.

[16] JCPDS-ICDD Card N 42-342

[17] J.-C. Grenier, S. Ghodbane, G. Demazeau, M. Pouchard and P. Hagenmuller, Mat. Res. Bull. **14**, 831 (1979).

[18] S.E. Dann and M.T. Weller, J. Solid State Chem. **115**, 499 (1995).

[19] V.V. Kharton, P.P. Zhyk, A.A. Troyan, T.E. Zhabko, A.A. Vecher, Neorgan. Mater. **27**, 2610 (1991).

[20] JCPDS-ICDD Card N 42-337.

Paper presented at the 5th Euroconference on Solid State Ionics, Benalmádena, Spain, Sept. 13-20, 1998.

Manuscript rec. Aug. 15, 1998; acc. Sept. 14, 1998.